CHEMISTRY OF MATERIALS

pubs.acs.org/cm

Article

Assembly of Linked Nanocrystal Colloids by Reversible Covalent Bonds

Manuel N. Dominguez, Michael P. Howard,[‖] Josef M. Maier,[‖] Stephanie A. Valenzuela,[‖] Zachary M. Sherman,[‖] James F. Reuther, Lauren C. Reimnitz, Jiho Kang, Shin Hum Cho, Stephen L. Gibbs, Arjun K. Menta, Deborah L. Zhuang, Aevi van der Stok, Sarah J. Kline, Eric V. Anslyn,* Thomas M. Truskett,* and Delia J. Milliron*

Cite This: *Chem. Mater.* 2020, 32, 10235−10245

Read Online

ACCESS | Metrics & More | Article Recommendations | Supporting Information

ABSTRACT: The use of dynamically bonded molecules designed to reversibly link solvent-dispersed nanocrystals (NCs) is a promising strategy to form colloidal assemblies with controlled structures and macroscopic properties. In this work, tin-doped indium oxide NCs are functionalized with ligands that form reversible covalent bonds with linking molecules to drive assembly of NC gels. We monitor the gelation by using small angle X-ray scattering and characterize how changes in the gel structure affect the infrared optical properties arising from the localized surface plasmon resonance of the NCs. The assembly is reversible because of the designed linking chemistry, and we disassemble the gels using two strategies: addition of excess NCs to change the ratio of linking molecules to NCs and addition of a capping molecule that displaces the linking molecules. The assembly behavior is rationalized using a thermodynamic perturbation theory to compute the phase diagram of the NC−linking molecule mixture. Coarse-grained molecular dynamics simulations reveal the competition between the loop and bridge linking motifs essential for understanding NC gelation. This combined experimental, computational, and theoretical work provides a platform for controlling and designing the properties of reversible colloidal assemblies that incorporate NC and solvent compositions beyond those compatible with other contemporary (e.g., DNA-based) linking strategies.

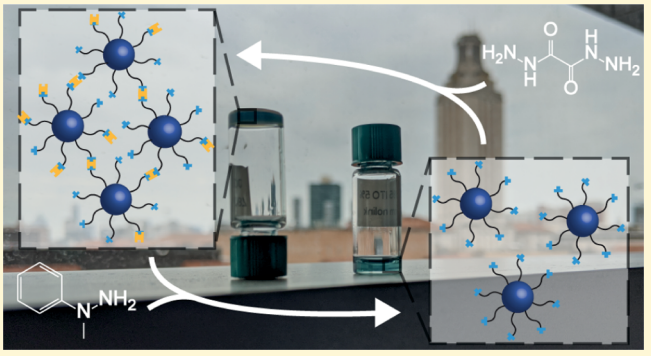

INTRODUCTION

Colloidal inorganic nanocrystals (NCs) are solvent-dispersible particles often exhibiting distinctive optical properties that depend on their synthetically tunable sizes and compositions.[1−5] Assemblies of NCs such as superlattices or gels reflect the properties of their constituent NCs, modified by interactions between the NCs that are absent or negligible in the dispersion, resulting in broad tunability based on the assembled structure.[6−15] These interactions are strongest between NCs that are close together in the assembly,[4,10,11,13,16,17] so the material's properties are sensitive to the number of nearest neighbors per NC (valence). Low NC density, porous gel assemblies have limited valence and promise tunability of valence-dependent material properties that are not typically possible in denser assemblies such as superlattices.[7−9,18]

Several strategies have been developed to produce NC gels, including ligand removal, direct chemical or physical bonding, and linking NCs with an intermediate.[7−9,19−25] By displacing surface-bound ligands that stabilize the NCs, a dispersion can become unstable with respect to aggregation and arrest in a gel network;[8,26,27] however, this process is typically irreversible, is difficult to control, and offers limited rational tuning of the network structure. Alternatively, the assembly can be driven by direct bonding between surface-bound ligands on different NCs, for example, through hybridization between NCs functionalized with complementary single-stranded DNA, though such direct bonding makes it difficult to control valence and dense aggregates typically form in preference to gels.[25,28−32] The valence can be controlled microscopically by limiting bonding to small numbers of "patches" on each particle,[33−35] but synthetic techniques for making patchy colloidal particles (∼1 μm diameter) do not easily translate to small NCs (∼10 nm diameter). Better control over NC valence can be achieved by using a bifunctional linking molecule (linker) that mediates bonding between the surface-

Received: October 25, 2020
Revised: November 5, 2020
Published: November 18, 2020

https://dx.doi.org/10.1021/acs.chemmater.0c04151
Chem. Mater. 2020, 32, 10235−10245

bound ligands.[19,20,36−39] With a linker, the NC assembly can be manipulated not only microscopically by design of the linker but also macroscopically by adjusting the linker concentration,[40] all without synthetically modifying the NCs themselves. Moreover, dynamically reconfigurable, or even reversible, NC gel assemblies can be made if reversible linking chemistries are used.[20,21,41] Previous examples that explored related concepts experimentally include cation-linked gels of anionically functionalized semiconductor NCs and DNA-functionalized gold nanoparticles assembled with complementary DNA linkers.[19−23,28,29,42−44]

Dynamic covalent bonding (DCB) presents a particularly compelling opportunity to engineer reconfigurable gel assemblies of NCs. DCB is compatible with a variety of solvent environments and NC compositions through the extensive organic synthetic toolbox[45−49] for creating DCB-functionalized ligands that bind NC surfaces. In contrast, DNA-mediated assembly has only been demonstrated in aqueous environments over a narrow temperature range and is restricted mostly to gold and silver particles.[28,29,38−40,50] The reversibility of DCB has been used to create self-healing, responsive, and reconfigurable polymer networks, whose links are dynamic.[44,45,51,52] When used to mediate attractions between NCs, DCB is expected to favor structures that tend toward equilibrium rather than becoming kinetically arrested, allowing thermodynamic principles to be leveraged to predict and design the phase behavior of NC assemblies. DCB has been incorporated in direct NC-to-NC bonding strategies using metal NCs functionalized with ligands bearing complementary DCB pairs, and these assemblies were shown to be reversible with the introduction of a competing molecule.[24] However, these studies produced only dense aggregates and did not report controlled assembly of percolated structures such as gels.[24,25]

Here, we exploit DCB in a facile linking assembly strategy for gelation using an aldehyde−hydrazide bonding pair. Specifically, we use DCB ligands and linkers to induce controlled assembly of tin-doped indium oxide (ITO) NCs into gels, guided by theoretical predictions of phase behavior and rationalized by simulations. The percolated networks of NCs are visualized by electron microscopy and structurally analyzed by small angle X-ray scattering (SAXS). As in prior examples of gold nanoparticle assembly,[17,53−55] ITO NCs exhibit a strong modulation of optical response upon assembly due to coupling of the localized surface plasmon resonance (LSPR) between neighboring NCs. Unlike gold, ITO resists irreversible fusing upon assembly,[56,57] so that the gels can be disassembled by leveraging the dynamic bonding equilibria linking the neighboring NCs in the network.

EXPERIMENTAL SECTION

NCs were synthesized by the modification of a slow injection method by the Hutchison group.[58] Briefly a metal precursor solution (4.75 mmol In(III)acetate, 0.25 mmol Sn(IV)acetate, and 10 mL oleic acid) was slow injected into 13 mL of oleyl alcohol held at 290 °C under an inert atmosphere. After the reaction, the NCs were washed five times with ethanol and redispersed in hexane. The ligands were synthesized using microwave-assisted solid-phase peptide synthesis followed by the solid-phase copper-catalyzed azide alkyne cycloaddition (SP-CuAAC) to add the DCB functionality. Standard Fmoc/*t* Bu protection strategies were used and deprotected using piperidine in dimethylformamide (DMF). DIC/Oxyma was used for amide coupling conditions. All ligands were synthesized at a 0.25 mmol scale using D-wang resin. The resulting resin was washed and dried under vacuum prior to SP-CuAAC. The dried resin was subjected to SP-CuAAC conditions previously described in the literature with 4-ethynylbenzaldehyde or 4-phenyl-1-butyne.[59] Once the DCB-functionalized ligand was cleaved from the resin and precipitated with ether, the resulting crude powder was purified using high-performance liquid chromatography. Liquid chromatography−mass spectrometry was used to determine the purity and identity of the products. Residual methanol was removed via rotary evaporation, and the water was lyophilized, yielding a white powder for each synthesized ligand. The NCs were functionalized using a direct ligand exchange method. Oleate-capped NCs in hexane were precipitated with ethanol and taken up in a polar ligand solution (0.01 M ligand in DMF) by sonication. The NCs were then precipitated using an ethanol/hexane (1:1) mixture and redispersed in neat DMF. The NCs were assembled with the addition of oxalyldihydrazide at various linker to NC concentrations. The solutions were lightly agitated upon mixing and monitored with SAXS for each concentration and over time.

Fourier-transform infrared (FTIR) measurements were conducted using a Bruker VERTEX 70 FTIR at 4 cm^{-1} resolution. Dynamic light scattering (DLS) measurements were performed on a Zetasizer Nano ZS with samples at dilute concentrations (0.1 mg/mL). SAXS samples were prepared in a capillary tube and flame-sealed. SAXS measurements were performed in the transmission configuration on a SAXSLAB GANESHA. Measurements were taken at regular intervals over the period of a month. For scanning transmission electron microscopy (STEM), samples were prepared by drop-casting NC dispersions onto carbon-coated 400 mesh copper grids, and imaging was performed in a Hitachi S5500 scanning electron miscroscope. Thermogravimetric analysis (TGA) was carried out using a Mettler Toledo TGA 2, and samples were loaded onto ceramic crucibles and dried under vacuum. Nuclear magnetic resonance (NMR) samples were prepared in a glovebox with an inert atmosphere using d 7-DMF. ^{1}H and ^{19}F NMR spectra were acquired on a MR400 system with a 400 MHz magnet and an OneNMR probe with Protune accessory. All NMR data were processed with the Mestrenova software package.

We developed a physical (bead−spring) model[60−63] for the NC−linker mixtures based on our previous theoretical efforts[33,36] and recent studies of gel-forming DNA nanostars.[64] Theoretical spinodal boundaries were computed with respect to the NC volume fraction and the linker-to-NC ratio using Wertheim's first-order thermodynamic perturbation theory (TPT).[65−69] Assembly of the NCs was simulated using LAMMPS (22 Aug 2018),[70] and various linking motifs, including some neglected by the theory, were quantified.

Complete details of the methods and materials are given in the Supporting Information.

RESULTS AND DISCUSSION

Ligand Design and Nanocrystal Functionalization. NC ligands bearing DCB groups were conveniently synthesized with a peptide synthesizer using established techniques for peptide synthesis and click chemistry (Figure 1a).[59,71−74] The ligands were designed with terminal functional groups to facilitate NC assembly, tethered to a NC surface-binding tricarboxylate domain by an ethylene glycol-based polyamide backbone (Figure 1b). The backbone confers solubility in the solvent we used, DMF, while the tridentate carboxylate binding domain is designed to have a high equilibrium constant for adsorption at the NC surface, avoiding ligand desorption by analogy with the stable complexation of metal ions by multidentate ligands.[75−77] In this work, we utilized the aldehyde−hydrazide DCB pairing, with ligands formed via copper-catalyzed "click" reactions between the resin-bound, azide-functional polyamide ligands and aldehyde alkynes (*p*-ethynylbenzaldehyde) as confirmed by liquid chromatography−mass spectrometry (LC−MS; Figure S1). These aldehyde functions can react with hydrazide groups on the linkers to

https://dx.doi.org/10.1021/acs.chemmater.0c04151
Chem. Mater. 2020, 32, 10235−10245

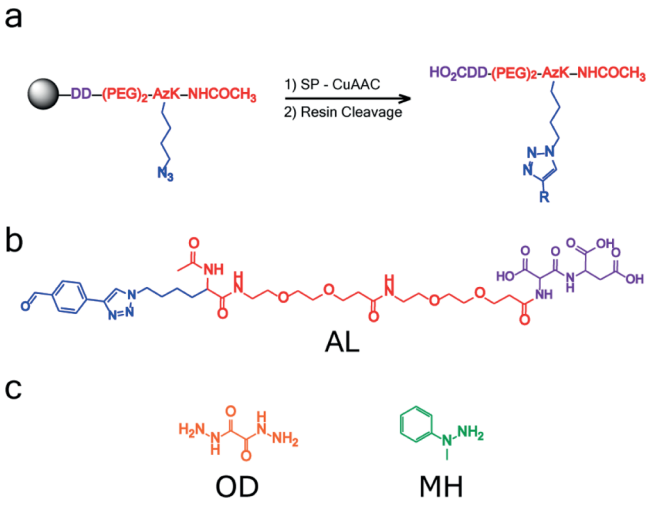

Figure 1. Ligand design and synthesis (a) Synthetic scheme for the functionalized ligands. (b) Structure of the aldehyde-functionalized ligand used in this study (**AL**) with different colors used to highlight ligand domains: (purple) attachment to NC, (red) assists in NC dispersibility, and (blue) functionalized domain for guided assembly. (c) Linker oxalyldihydrazide (**OD**) and the capping molecule 1-methyl-1-phenyl hydrazide (**MH**).

form hydrazone DCB products.[78] The versatility of this ligand synthesis approach allows substitution of the functional end group with other DCB groups, tuning of the backbone chemistry and length, and modification of the NC binding domain to match different NC compositions. The linker and capping molecule, oxalyldihydrazide (**OD**) and 1-methyl-1-phenylhydrazine (**MH**), respectively (Figure 1c), are complementary to the functional DCB aldehyde end group in the ligand (Figure 1b) and provide the molecular control for assembly and disassembly. A similarly synthesized ligand with a benzyl end group (**BL**) was made for assembly control experiments (Figure S1).

ITO NCs were synthesized using a slow growth technique[58] that produces a highly uniform size distribution of NCs capped with oleate ligands, which were then partially exchanged with aldehyde-functionalized ligands (**AL**). The high binding affinity made direct functionalization by mass action effective, and the previously cloudy suspension of NCs became clear following brief agitation. STEM images of the NCs before and after functionalization show no change in NC size or morphology (Figure 2a,b). The NC sizes found by analysis of STEM and SAXS were in close agreement [diameter 12.2 ± 1.0 nm based on SAXS analysis (Figure S2)]. The presence of bound **AL** together with native oleate ligands was apparent in the ^{1}H NMR spectrum of a functionalized NC dispersion. The peaks at 8.98 ppm (amine) and 10.26 ppm (aldehyde) are clear signatures of **AL**, while the peak at 5.56 ppm is slightly shifted and weaker but still present and characteristic of the oleate ligand (Figure 2c). These peaks are consistent with the bound state of the ligands, as they are significantly broadened and shifted slightly downfield compared to the free ligands.[79−83]

To further analyze the ligand functionalization of the NCs and assess their optical properties, FTIR spectra were taken of NC solvent dispersions before and after functionalization with **AL**. The strong LSPR absorption at 4790 cm^{-1} was nearly unchanged from the as-synthesized NCs capped only with oleic acid, suggesting that the NCs were well-dispersed (Figure 2d). Aggregation would be expected to red-shift and broaden the spectrum.[84−86] The fingerprint region of the FTIR was examined for evidence of **AL** functionalization. The **AL**-NCs exhibit a strong and broad carbonyl stretch (1670 cm^{-1}), an aldehyde C−H bending mode (1380 cm^{-1}), and a C−O stretch arising from the ethylene glycol backbone (1090 cm^{-1}) (Figure S3). To assess the average number of **AL** molecules bound to each NC, we saturated the aldehyde groups with a fluorine-tagged hydrazine to facilitate quantitative analysis by ^{19}F NMR spectroscopy (Figure S4). Specifically, 4-fluorophenylhydrazine was introduced at about 500:1 number ratio with

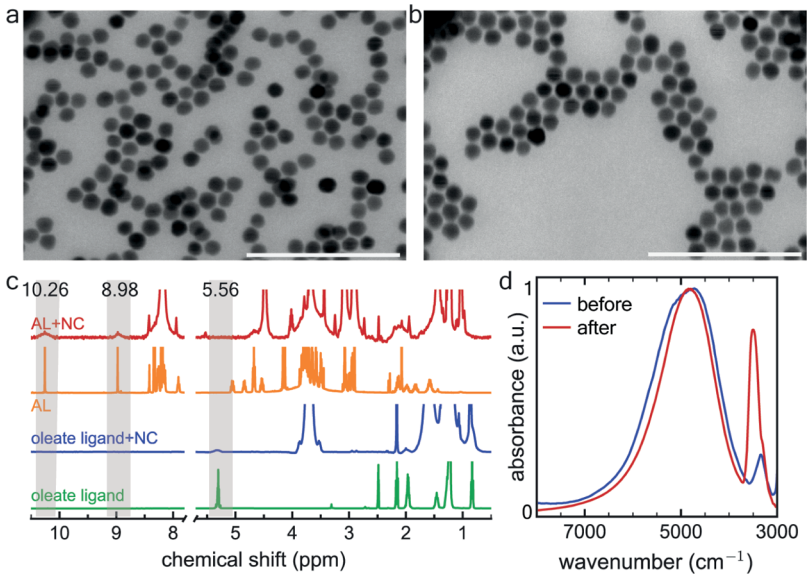

Figure 2. Characterization of **AL**-functionalized NCs. STEM images of (a) NCs capped with native oleate ligands and (b) with **AL** (scale bars are 100 nm). (c) ^{1}H NMR spectra of NCs before and after ligand exchange (blue and red, respectively) show broadened peaks (shaded) characteristic of oleate ligands (green) and **AL** (orange). (d) LSPR absorption spectra of NC dispersions before (in hexane, blue) and after **AL** functionalization (in DMF, red). The peak near 3400 cm^{-1} is due to adventitious water.

https://dx.doi.org/10.1021/acs.chemmater.0c04151
Chem. Mater. 2020, 32, 10235−10245

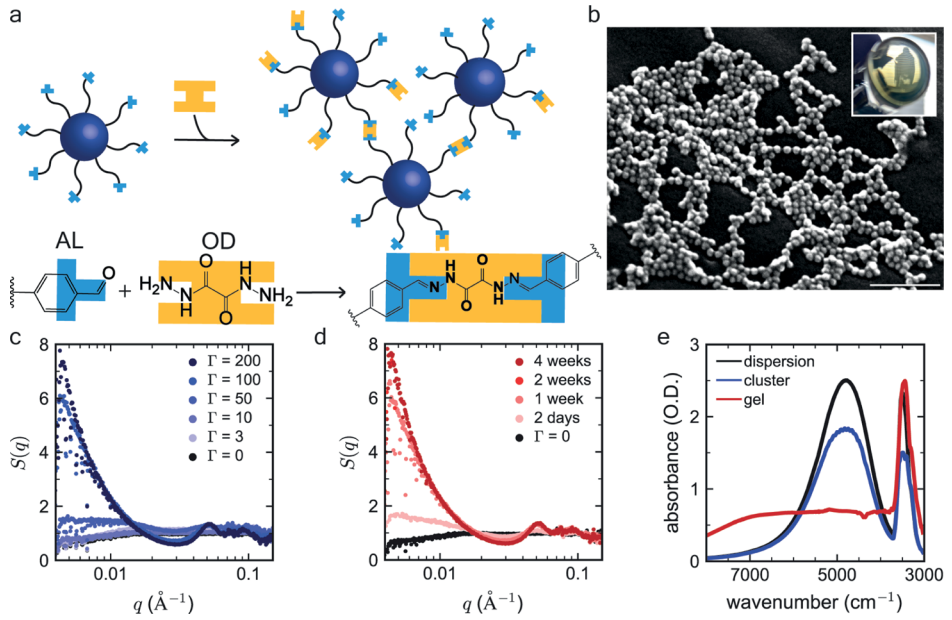

Figure 3. DCB-linker assembly of ITO NCs. (a) Schematic of the linking process creating a bond between aldehyde ligand (**AL**)-functionalized NCs with oxalyl dihydrazide (**OD**). (b) SEM of a linker-to-NC ratio Γ = 200 gel (scale bar, 100 nm), pictured in the inset photo. (c) SAXS structure factor of samples 2 weeks after adding **OD** at varying Γ. (d) SAXS structure factor of Γ = 100 samples over time after adding **OD**. (e) FTIR of the LSPR response of a discrete NC dispersion compared to the cluster (Γ = 50) and gel (Γ = 200) samples.

the NCs, in excess of the expected concentration of bound **AL**, and the NCs possessing the resulting fluorinated derivatized hydrazone ligands were washed multiple times using deuterated solvents. The fluorine peak for the free 4-fluorophenylhydrazine (127.4 ppm) shifts and broadens upon bonding with the surface-bound **AL** (125.3 ppm). The average number of ligands bound to each NC was identified by comparing the concentration of NCs (determined by weight) to the calculated amount of **AL** found by ^{19}F NMR. The number of bound ligands was also independently assessed by TGA of NCs before and after **AL** functionalization (Figure S5). Similar methods were used in previously reported DCB–NC systems to characterize the ligand shell.[24] Good agreement between ligand quantification by ^{19}F NMR and TGA indicated a mixed ligand shell of oleate ligands and **AL**, with an average number of 152 ± 20 and 135 ± 33 **AL** per NC (determined by ^{19}F NMR and TGA, respectively). This large number of ligands would not limit valence in a direct NC-to-NC bonding scheme. However, as we now describe, the controlled addition of a limited amount of the complementary dihydrazide linker **OD** allows us to control NC valence and gelation.

Nanocrystal Assembly. A bifunctional linker molecule was added to dispersions of the **AL**-functionalized NCs (volume fraction 0.004) to induce aggregation, assembly, and ultimately gelation (Figure 3a). Specifically, small amounts of **OD** were added to dispersions of NCs in DMF to create mixtures with linker-to-NC ratios (Γ) between 1 and 200. For Γ = 0 up to Γ = 50, no visual changes were apparent, and all samples flowed easily in the vials when titled. DLS on diluted aliquots revealed only minor aggregation with a systematic increase in hydrodynamic radius up to about twice the size of an individual NC for Γ = 50 (Figure S6). Higher concentrations of linker brought about more substantial changes in the dispersions, with the Γ = 100 and 200 samples forming two phase systems with a soft gel and free flowing clear solvent layer after 1 month or less (Figure S7). SEM imaging of a dried gel revealed branching chains of NCs forming an open porous network between denser NC clusters (Figure 3b).

NC assemblies across the full range of linker concentrations were monitored, and their structures were assessed by using SAXS, which unlike DLS can be carried out without perturbing the mixtures by dilution. To isolate the structure factor $S(q)$, which characterizes the mesoscale organization of the NCs, the scattering intensity $I(q)$ was divided by the form factor extracted from a dilute NC dispersion (see discussion in the Supporting Information). No significant changes to $S(q)$ are observed for samples below Γ = 50 when compared to the control sample without a linker, suggesting little (if any) NC assembly or aggregation occurs (Figure S8). Similarly, a control sample with Γ = 200 and NCs capped with **BL** instead of **AL** showed no signs of aggregation by eye or SAXS (Figure S9). For the **AL**-functionalized NCs, a peak at high q (q = 0.051 Å^{-1}) appears for Γ ≥ 50 and becomes more pronounced with time, growing more rapidly for a higher Γ. Based on the corresponding length scale ($l \sim 2\pi/q$ = 12.3 nm) and consistent with the interpretation in previous reports, this high q peak is attributed to a contact peak arising from the local packing of NCs as they bond and form aggregates.[43,87,88] The Γ = 100 sample showed signs of aggregation within 2 days of the introduction of linker to the NC dispersion (Figure 3c). Cluster aggregation is expected to produce a peak in $S(q)$ whose position corresponds to the characteristic size of the clusters, so a broad peak in the low q region indicates a heterogeneous distribution of cluster sizes.[73,89] A broad peak at low q (starting at $q \leq 0.03$ Å^{-1}) was observed after 2 days, shifting to lower q over time, consistent with the formation of larger clusters and, ultimately, percolated networks spanning the entire macroscopic sample and inhibiting flow. The magnitude of $S(q)$ at the lowest measured q increases over time, stabilizing by 4 weeks at a value comparable to previously reported values for colloidal gels.[90,91]

https://dx.doi.org/10.1021/acs.chemmater.0c04151
Chem. Mater. 2020, 32, 10235−10245

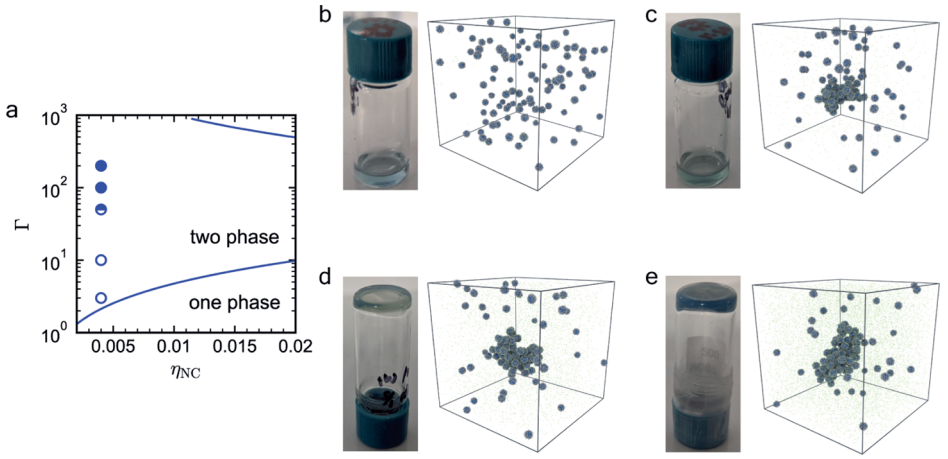

Figure 4. Theory and simulation of NC−linker phase behavior. (a) Theoretically predicted spinodal boundary compared with experimentally characterized flowing dispersions (open circles), aggregates (half-filled circle), and gels (filled circles). The single-phase dispersion is thermodynamically unstable for Γ between the branches. Photographs of experiments and simulation snapshots are shown for linker-to-NC ratios (b) Γ = 10, (c) 50, (d) 100, and (e) 200.

The functional form of $S(q)$ in the low q region contains information regarding the mesoscale structure of the NC assembly, indicating that the gels are formed by sample-spanning networks of linked NCs. The Porod region of the S(q) data exhibits power-law scaling, $I(q) \propto q^{-D_f}$, for fractal networks such as colloidal gels[7,92−94] and for mass fractals, with fractal dimension (D_f) at or above 1.8. The SAXS patterns for our gel samples all exhibit a single Porod region for $q < 0.03$ Å^{-1} with the Γ = 100 and 200 samples having $D_f = 1.8$ and 1.9, respectively (Figure S10). These values are at the low end of the gelation range of $1.8 \leq D_f \leq 3$ typically reported for colloidal gels, but indicate that our samples are gels and not dense precipitates.[77,79−96] The value of D_f can reflect the kinetic mechanism underlying gelation, with diffusion-limited aggregation of colloids reported to produce networks with D_f as low as 1.8.[79,80] Diffusion-limited aggregation tends to produce stringy networks, consistent with the appearance of our samples (Figure 3b).[79] Reaction-limited aggregation produces more globular network structures, with D_f typically in the range of 2.1−2.2.[79−81] These values are sufficiently close to those we observed, suggesting that the underlying mechanism controlling gelation of DCB-linked NCs warrants further investigation.

FTIR analysis before and after assembly indicates that aggregation is specifically induced by hydrazone bond formation between **AL** and the **OD** linkers. In the gels, a hydrazone C═N stretch emerges (1690 cm^{-1}), while the aldehyde C−H bending peak (1380 cm^{-1}) decreases in intensity and the amine C−N bending increases (1250 cm^{-1}) (Figure S11). The infrared optical response of the NCs also changes substantially as the NCs are linked. The LSPR of a linked NC gel is broadened, and the peak intensity is diminished when compared to the discrete NC dispersion (Figure 3e). Broadening due to NC−NC LSPR coupling has been reported previously in gel and thin film assemblies of ITO NCs, though the extent of broadening is greater in this study.[7,69,97] In samples that remain free-flowing but where SAXS suggests cluster formation, for example Γ = 50, the LSPR is slightly broadened, as expected for LSPR coupling between nearby NCs (Figure 3e).[1,7,71] The much broader extinction spectrum for the gel may be a result of not only increased coupling of neighboring NCs, but also the increased contribution of optical scattering by large aggregates in the network. The optical extinction of individual NCs is dominated by absorption, rather than scattering, because the NCs are too small to scatter light at these long infrared wavelengths.[98] As aggregates grow, they form large clusters able to scatter infrared light more efficiently, which can contribute to peak broadening.[63,64] Further, heterogeneity in cluster size within the network would also contribute to peak broadening. STEM of our gels reveals porous networks and portions of the assembly that are densely packed with NCs (Figures 3b and S12). Such extended, dense aggregates could support collective LSPR modes, similar to array modes in patterned or self-assembled arrays of plasmonic nanostructures.[69,70] In gels, the heterogeneous nature of the aggregates would support a wide variation of coupled, delocalized modes with different peak energies and linewidths that broaden the observed far-field spectrum.[51,99,100] The dramatic change in the optical spectrum upon assembly suggests that ITO NC gels hold promise as dynamic or responsive infrared optical materials.

Thermodynamic Driving Force for Assembly. To rationalize our experimental observations, we computed theoretical spinodal boundaries for the mixture with respect to the NC volume fraction η_{NC} and the linker-to-NC ratio Γ (Figure 4a) using first-order TPT.[65−69] When Γ increases above the spinodal boundary, the single-phase mixture becomes thermodynamically unstable to fluctuations in the concentration of NCs and phase separation becomes spontaneous. One phase is rich in NCs, and in experiments and simulations, it tends to arrest as a gel. Qualitatively, this transition from a single dispersed phase to a gel is also observed in our experiments, where the mixtures remained as flowing dispersions for Γ < 50, but formed large aggregates or gels for Γ ≥ 50. However, this transition occurred at a much higher linker-to-NC ratio than predicted by TPT (Γ = 2.1).

We hypothesized that this discrepancy might be due to the formation of cycles or "loops" in the NC−linker network in the experiments, in violation of one of TPT's key simplifying assumptions.[93] Loops can emerge, for example, when two ligands on the same NC are linked to each other via **OD**, or when multiple links form between the same two neighboring NCs. Based on our prior theoretical study,[33] these motifs tend

https://dx.doi.org/10.1021/acs.chemmater.0c04151
Chem. Mater. 2020, 32, 10235−10245

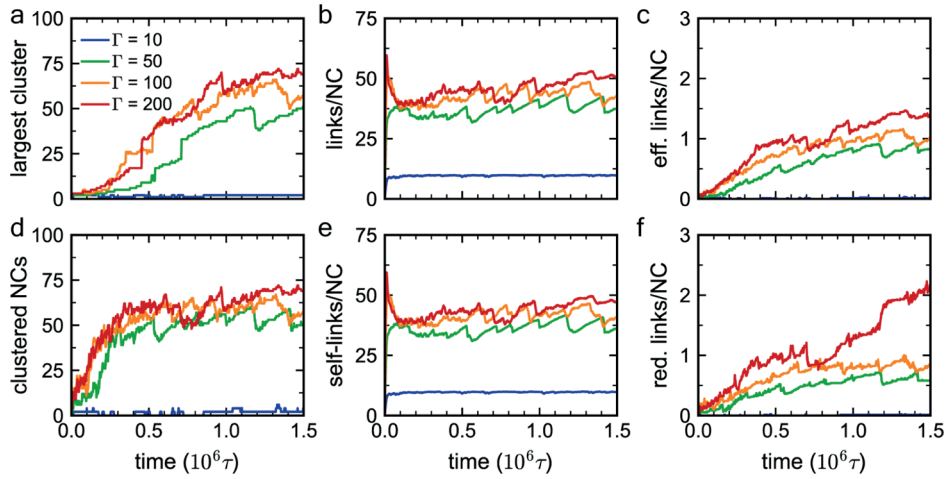

Figure 5. Analysis of simulated NC−linker structures. (a) Largest NC cluster size and (d) total number of NCs in clusters as a function of simulation time for varied linker-to-NC ratios Γ. Number of linkers (per NC) forming (b) link between any two ligands, (c) effective (unique) link between two NCs, (e) self-link between two ligands on the same NC, and (f) redundant link between two NCs. The total number of NCs is 100.

to hinder gelation by "wasting" linkers that could otherwise form links that further extend the NC network and seem to cause TPT to underestimate the amount of linkers required for phase separation. We suspected that a large fraction of linkers form loop motifs in the NC−linker samples and that this might cause substantial deviations from the TPT predictions. To test this hypothesis, we performed molecular simulations that used the same model interactions as TPT but allowed for the formation of loop structures. We monitored the formation of NC clusters at Γ = 10, 50, 100, and 200 (Figure 5a,d). In agreement with the experiments, the NCs formed a single large aggregate indicative of a tendency to phase separate for Γ ≥ 50, but remained dispersed for Γ = 10, forming a few dimers at most. The aggregates were visually apparent in snapshots of the simulations (Figure 4b−e) and tended to be larger for higher Γ(Figure 5a). Our simulations were computationally limited to 100 NCs, so we were unable to simulate the fractal gel network that forms over larger length scales in the experiments.

We quantified the different linking motifs occurring in simulations (Figure 5b,c,e,f) to rationalize the disagreement between the experiments and the theoretical phase boundaries. The linker almost instantaneously bonds with the NC-bound ligands (Figure 5b), and an overwhelming fraction of these form self-links between ligands on the same NC (Figure 5e), particularly for the mixtures with larger Γ. Rapid formation of self-links is consistent with the studies of kinetics of hydrazone formation.[58,62,101,102] The system is energetically driven toward bond formation so that both ends of each linker quickly attach to any nearby available ligands. As the simulations progress, the number of unique (or "effective") links between NCs gradually increases (Figure 5c) for the mixtures that aggregated. In contrast to the self-links, the effective links form slowly because they require at least two NCs or NC clusters to diffuse near each other and subsequently link. Making the link to a neighboring NC may also require one end of the linker to first release from a self-link. A small number of redundant links (multiple links between the same NCs) also formed between NCs (Figure 5f), along with the effective links, constituting another potential waste of linker. However, the redundant links help stabilize the aggregates against bond breaking events due to avidity effects wherein multiple bonds between a pair of species provide stabilization even beyond their additive individual bond strengths. Overall, though, the number of redundant links was small compared to the number of self-links. Indeed, self-links accounted for roughly 95% of all links formed. This factor is similar to the discrepancy between the predicted and observed Γ required for phase separation and might be used to crudely renormalize Γ to account for the "wasted" linkers. Taken together, the simulations strongly suggest that self-links play a significant role in determining the amount of linkers required for gelation compared to theoretical predictions that do not account for them.

One potential design strategy to make self-linking less likely is to reduce the number of functionalized ligands per NC. TPT predicts similar low-Γ spinodal branches when the number of functionalized ligands is modestly decreased (Figure S14). We performed additional simulations at a constant linker-to-NC ratio Γ = 50 where now only 25, 50, or 75% of the ligands per NC were considered functionalized and able to form bonds with the linkers. We found that the numbers of clustered NCs (Figure S15), effective links, and redundant links were comparable in all cases, but the number of total links and self-links decreased with decreasing fractions of functionalized ligands. The largest aggregate size was comparable between the 50, 75, and 100% functionalized cases, but was much smaller in the 25% case. However, even the 25% case may be slowly progressing toward a similar assembled structure, considering that the total number of clustered NCs is comparable and that the largest cluster size continues to slowly increase throughout the time accessible in the simulations.

These simulations agree with our expectations that the phase behavior should be controlled by an effective number of linkers in the mixture (excluding those lost to self-links), suggesting that reducing the number density of **AL** on the NCs may give a path to achieve the same assembly behavior using fewer **OD** linkers. Indeed, the fraction of unbound linkers in the simulations increases with the decreasing number of functionalized ligands (Figure S16), so a lower linker concentration might achieve a comparable assembly. Importantly for this strategy, only the average number of functionalized ligands need be reduced, for example, by mixing passive ligands and **AL** on the surface, while precise control over the number of aldehyde groups at the single-NC level is unnecessary. Control

https://dx.doi.org/10.1021/acs.chemmater.0c04151
Chem. Mater. 2020, 32, 10235−10245

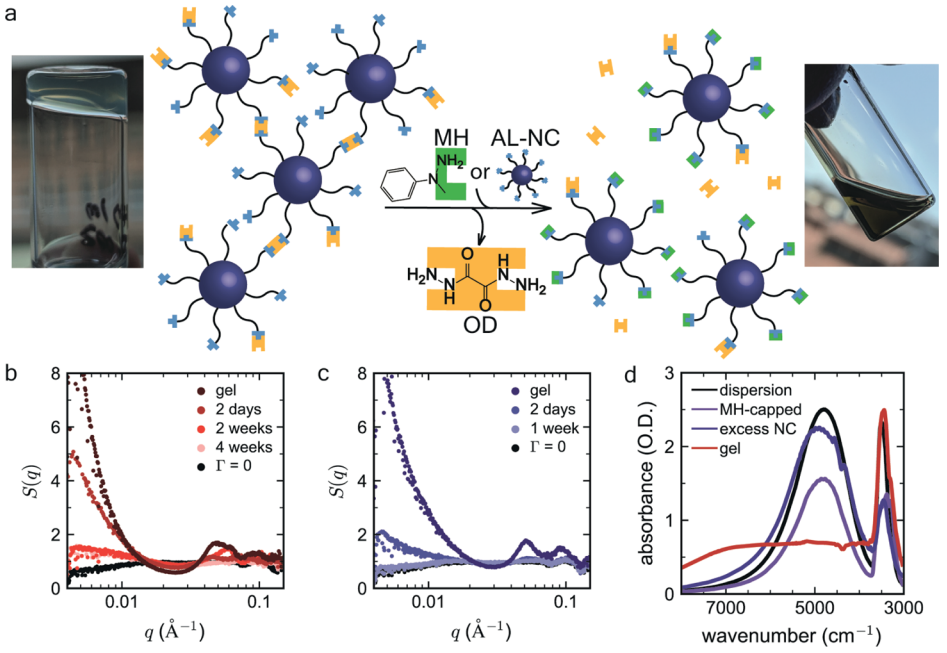

Figure 6. Disassembly of NC gels. (a) Schematic of disassembly from a gel (photo on left) to a free-flowing dispersion instigated by addition of a capping molecule (**MH**) or excess **AL** capped NCs. (b) SAXS structure factor tracking the disassembly of a gel using **MH** over 1 month. (c) SAXS structure factor for disassembly with excess **AL**-NCs; brief sonication was used to break up the gel. The gel did not reform and SAXS shows minimal evidence of aggregation after 1 week. (d) LSPR spectra of the **AL**-NC dispersion, NC gel, and both samples after gel reversal.

over the average coverage is much more experimentally accessible than previous efforts to make patchy NCs with discrete, specific numbers of DNA ligands, for example.[103] However, we note that there are other potential strategies that might similarly reduce self-linking, including modifying the ligand flexibility or using an asymmetric linker with differing DCB groups on either end. In the future, we intend to explore the advantages and disadvantages of these strategies for controlling assembly.

Reversibility. Because the linkers form reversible covalent bonds and ITO NCs resist fusing, the calculated phase diagrams may provide guidance on conditions suitable for reversing the gelation process, for example, through changes in **OD** to NC ratios, laying the foundation for the development of responsive NC assemblies. Gel disassembly is predicted when the macroscopic NC or linker concentration is changed to navigate outside the spinodal boundary. To realize this experimentally, the system needs to be able to re-establish equilibrium, which is possible using our linking strategy because of the dynamic nature of the hydrazone bonds (Figure 6a). The introduction of molar-excess amounts of a capping molecule, 1-methyl-1-phenylhydrazine (**MH**), reverses gelation within 2 days after its addition (Figure 6b). The monofunctional hydrazine competes with the linker for bonding with the aldehyde terminus of the ligands and can disrupt the NC network by breaking the linkages. Analogous breaking of DCB-linked polymer networks[43,45] has been demonstrated by introducing a small molecule that displaced the bonded functional groups on the neighboring polymer chains.[47,48,104,105]

In our linked NC gels, the capping molecule **MH** disrupted the network, recovering a free-flowing dispersion. SAXS revealed that the gel reversal process did not result in a dispersion of completely discrete NCs. Instead, the structure factor at low $q < 0.01$ Å^{-1} retains a weak peak, suggesting the presence of NC clusters, similar to $S(q)$ for the $\Gamma = 50$ sample. The low q intensity continues to diminish from 2 days to 4 weeks after addition of the molecular capping agent. The dispersion flows easily and is clear, with a slight yellow-orange tinge due to the addition of **MH**, which is yellow-orange itself before addition.

The second method for gel reversal that we tested was to introduce excess **AL**-functionalized NCs to the gel sample. A volume of this NC dispersion was added, keeping the NC volume fraction fixed, while changing from $\Gamma = 200$ to $\Gamma = 30$, which was below the threshold we observed above for gelation. Initial observation showed no apparent change to the gel after leaving it undisturbed for 2 weeks, so the sample with excess NCs and a control gel sample were subjected to a brief sonication (10 min) to break the gels apart and attempt to overcome any initial kinetic barriers to redispersion of the NCs. The gel control sample without **MH** or excess NCs, though initially broken apart by sonication, was found to reform a cohesive gel over a few days. By contrast, the sample with excess NCs added remained dispersed. Over the course of a week, however, a small portion of that sample aggregated and precipitated. The structure factor of the dispersed portion showed no evidence of residual or renewed NC aggregation after 1 week (Figure 6c). For either gel reversal strategy, conditions that minimize self-linking (e.g., diluting **AL** with passive ligands) may allow more complete redispersion because gels could be formed with far less linkers.

The chemical and thermodynamic strategies demonstrated for gel reversal suggest opportunities to design responsive optical materials if the LSPR signature of discrete NCs can also be recovered. Indeed, the absorption spectra of samples induced to disassemble by either approach are similar to the spectrum of the **AL**-functionalized NCs before assembly. The peak is again found at 4800 cm^{-1} with only minimal broadening and red shift (Figure 6d), consistent with slight

https://dx.doi.org/10.1021/acs.chemmater.0c04151
Chem. Mater. 2020, 32, 10235−10245

residual aggregation as suggested by the SAXS data. The recovery of the LSPR confirms that the NCs remain discrete within the gel assemblies and suggests opportunities for future development of switchable and chemically programmable optical materials based on the selectivity and the dynamic nature of DCBs[42,44,62,106] when applied to dispersions containing different optically active NC building blocks.

CONCLUSIONS

Reversible covalent bonding provides a platform where dynamic molecular links between colloidal NCs can be designed to realize theoretically predicted colloidal assemblies including gels. We have demonstrated this platform with a system of aldehyde-functional ligands (**AL**), prepared by a scalable process via peptide synthesis, including a solubilizing tether and a multidentate carboxylate binding domain suitable for metal oxide surfaces, applied to infrared-plasmonic ITO NCs. When paired with a bifunctional hydrazide linker (**OD**), the assembly behavior of the **AL**-functionalized NCs is rationally controlled by the **OD**-to-NC ratio Γ, as anticipated from theory. Quantitative discrepancy between the gelation threshold observed experimentally and the theoretically predicted spinodal boundary is attributed, based on the results of coarse-grained simulations, to the large fraction of linker molecules "wasted" in forming links between two ligands on a single NC (i.e., self-links). Nonetheless, the gelation can be largely reversed either by displacing linker−ligand bonds with capping molecules or by navigating across the spinodal boundary via linker dilution. Assembly and disassembly are accompanied by substantial changes in the infrared optical properties due to LSPR coupling between NCs in the gel network.

Because the aldehyde−hydrazide pair represents one among several tunable orthogonal reversible covalent (TORC) bonding pairs,[41,42,62,102] these results set the stage for diverse opportunities in programmable and reconfigurable optical materials based on TORC-linked NC networks. In addition to the metal oxide NCs studied here, we can adapt this system to a range of other NCs with interesting optical properties. In fact, using two orthogonal TORC pairs, mixtures of two types of NCs can be made to assemble independently of one another in the same mixture, as has been previously demonstrated for direct NC-to-NC bonding.[24] In our linker-mediated assembly approach, the NC networks can be tuned by modifying the properties (e.g., rigidity, solvent compatibility, and response to stimuli) of the linker molecules, surpassing the level of control in DNA-based assembly.[28,38,39,99,107] TORC chemistry is a powerful and tunable platform for linker-based NC assembly applicable over a range of solvent environments and temperatures. It opens up an avenue for development of NC materials whose macroscopic properties are responsive and adaptive based on nanoscale structural changes.

ASSOCIATED CONTENT

Supporting Information

The Supporting Information is available free of charge at https://pubs.acs.org/doi/10.1021/acs.chemmater.0c04151.

Details of the experimental methods (synthesis, functionalization, and assembly and disassembly) and the theoretical methods (model, TPT, and simulations) (PDF)

AUTHOR INFORMATION

Corresponding Authors

Eric V. Anslyn − *Department of Chemistry, University of Texas at Austin, Austin 78712-1589, Texas, United States;* orcid.org/0000-0002-5137-8797; Email: anslyn@austin.utexas.edu

Thomas M. Truskett − *McKetta Department of Chemical Engineering and Department of Physics, University of Texas at Austin, Austin 78712-1589, Texas, United States;* orcid.org/0000-0002-6607-6468; Email: truskett@che.utexas.edu

Delia J. Milliron − *Department of Chemistry and McKetta Department of Chemical Engineering, University of Texas at Austin, Austin 78712-1589, Texas, United States;* orcid.org/0000-0002-8737-451X; Email: milliron@che.utexas.edu

Authors

Manuel N. Dominguez − *Department of Chemistry, University of Texas at Austin, Austin 78712-1589, Texas, United States;* orcid.org/0000-0002-9606-9234

Michael P. Howard − *McKetta Department of Chemical Engineering, University of Texas at Austin, Austin 78712-1589, Texas, United States;* orcid.org/0000-0002-9561-4165

Josef M. Maier − *Department of Chemistry, University of Texas at Austin, Austin 78712-1589, Texas, United States*

Stephanie A. Valenzuela − *Department of Chemistry, University of Texas at Austin, Austin 78712-1589, Texas, United States;* orcid.org/0000-0002-0399-275X

Zachary M. Sherman − *McKetta Department of Chemical Engineering, University of Texas at Austin, Austin 78712-1589, Texas, United States*

James F. Reuther − *Department of Chemistry, University of Texas at Austin, Austin 78712-1589, Texas, United States*

Lauren C. Reimnitz − *McKetta Department of Chemical Engineering, University of Texas at Austin, Austin 78712-1589, Texas, United States*

Jiho Kang − *McKetta Department of Chemical Engineering, University of Texas at Austin, Austin 78712-1589, Texas, United States*

Shin Hum Cho − *McKetta Department of Chemical Engineering, University of Texas at Austin, Austin 78712-1589, Texas, United States;* orcid.org/0000-0002-0271-116X

Stephen L. Gibbs − *McKetta Department of Chemical Engineering, University of Texas at Austin, Austin 78712-1589, Texas, United States;* orcid.org/0000-0003-2533-0957

Arjun K. Menta − *Department of Chemistry, University of Texas at Austin, Austin 78712-1589, Texas, United States*

Deborah L. Zhuang − *Department of Chemistry, University of Texas at Austin, Austin 78712-1589, Texas, United States;* orcid.org/0000-0003-1806-2552

Aevi van der Stok − *Department of Chemistry, University of Texas at Austin, Austin 78712-1589, Texas, United States*

Sarah J. Kline − *McKetta Department of Chemical Engineering, University of Texas at Austin, Austin 78712-1589, Texas, United States*

Complete contact information is available at: https://pubs.acs.org/10.1021/acs.chemmater.0c04151

https://dx.doi.org/10.1021/acs.chemmater.0c04151
Chem. Mater. 2020, 32, 10235−10245

Author Contributions

[‖]M.P.H. and J.M.M. contributed equally. S.A.V. and Z.M.S. authors contributed equally.

Notes

The authors declare no competing financial interest.

■ ACKNOWLEDGMENTS

We would like to acknowledge the UT Mass Spectrometry Facility for their instrumental help and the UT NMR facilities for equipment use and assistance: NIH grant number 1 S10 OD021508-01. This work was primarily supported by the National Science Foundation through the Center for Dynamics and Control of Materials: an NSF Materials Research Science and Engineering Center (NSF MRSEC) under Cooperative Agreement DMR-1720595. This work was also supported by the NSF Graduate Research Fellowships DGE-1610403 (M.N.D. and S.V.), an Arnold O. Beckman Postdoctoral Fellowship (Z.M.S.), NSF (CHE-1905263), and the Welch Foundation (F-1848 and F-1696). E.V.A. acknowledges support from the Welch Regents Chair (F-0046). We acknowledge the Texas Advanced Computing Center (TACC) at The University of Texas at Austin for providing HPC resources.

■ REFERENCES

(1) Agrawal, A.; Cho, S. H.; Zandi, O.; Ghosh, S.; Johns, R. W.; Milliron, D. J. Localized Surface Plasmon Resonance in Semiconductor Nanocrystals. *Chem. Rev.* **2018**, *118*, 3121−3207.

(2) Alivisatos, A. P. Semiconductor Clusters, Nanocrystals, and Quantum Dots. *Science* **1996**, *271*, 933−937.

(3) Shamsi, J.; Urban, A. S.; Imran, M.; De Trizio, L.; Manna, L. Metal Halide Perovskite Nanocrystals: Synthesis, Post-Synthesis Modifications, and Their Optical Properties. *Chem. Rev.* **2019**, *119*, 3296−3348.

(4) Talapin, D. V.; Lee, J.-S.; Kovalenko, M. V.; Shevchenko, E. V. Prospects of Colloidal Nanocrystals for Electronic and Optoelectronic Applications. *Chem. Rev.* **2010**, *110*, 389−458.

(5) Murray, C. B.; Kagan, C. R.; Bawendi, M. G. Synthesis and Characterization of Monodisperse Nanocrystals and Close-Packed Nanocrystal Assemblies. *Annu. Rev. Mater. Sci.* **2000**, *30*, 545−610.

(6) Wang, D.; Yang, A.; Hryn, A. J.; Schatz, G. C.; Odom, T. W. Superlattice Plasmons in Hierarchical Au Nanoparticle Arrays. *ACS Photonics* **2015**, *2*, 1789−1794.

(7) Saez Cabezas, C. A.; Ong, G. K.; Jadrich, R. B.; Lindquist, B. A.; Agrawal, A.; Truskett, T. M.; Milliron, D. J. Gelation of Plasmonic Metal Oxide Nanocrystals by Polymer-Induced Depletion Attractions. *Proc. Natl. Acad. Sci. U.S.A.* **2018**, *115*, 8925−8930.

(8) Mohanan, J. L.; Arachchige, I. U.; Brock, S. L. Porous Semiconductor Chalcogenide Aerogels. *Science* **2005**, *307*, 397−400.

(9) Bigall, N. C.; Herrmann, A.-K.; Vogel, M.; Rose, M.; Simon, P.; Carrillo-Cabrera, W.; Dorfs, D.; Kaskel, S.; Gaponik, N.; Eychmüller, A. Hydrogels and Aerogels from Noble Metal Nanoparticles. *Angew. Chem., Int. Ed.* **2009**, *48*, 9731−9734.

(10) Ye, X.; Chen, J.; Diroll, B. T.; Murray, C. B. Tunable Plasmonic Coupling in Self-Assembled Binary Nanocrystal Superlattices Studied by Correlated Optical Microspectrophotometry and Electron Microscopy. *Nano Lett.* **2013**, *13*, 1291−1297.

(11) Tao, A.; Sinsermsuksakul, P.; Yang, P. Tunable Plasmonic Lattices of Silver Nanocrystals. *Nat. Nanotechnol.* **2007**, *2*, 435−440.

(12) Shevchenko, E. V.; Ringler, M.; Schwemer, A.; Talapin, D. V.; Klar, T. A.; Rogach, A. L.; Feldmann, J.; Alivisatos, A. P. Self-Assembled Binary Superlattices of CdSe and Au Nanocrystals and Their Fluorescence Properties. *J. Am. Chem. Soc.* **2008**, *130*, 3274−3275.

(13) Kim, S.-H.; Medeiros-Ribeiro, G.; Ohlberg, D. A. A.; Williams, R. S.; Heath, J. R. Individual and Collective Electronic Properties of Ag Nanocrystals. *J. Phys. Chem. B* **1999**, *103*, 10341−10347.

(14) Weidman, M. C.; Smilgies, D.-M.; Tisdale, W. A. Kinetics of the Self-Assembly of Nanocrystal Superlattices Measured by Real-Time in Situ X-Ray Scattering. *Nat. Mater.* **2016**, *15*, 775−781.

(15) Boneschanscher, M. P.; Evers, W. H.; Geuchies, J. J.; Altantzis, T.; Goris, B.; Rabouw, F. T.; van Rossum, S. A. P.; van der Zant, H. S. J.; Siebbeles, L. D. A.; Van Tendeloo, G.; Swart, I.; Hilhorst, J.; Petukhov, A. V.; Bals, S.; Vanmaekelbergh, D. Long-Range Orientation and Atomic Attachment of Nanocrystals in 2D Honeycomb Superlattices. *Science* **2014**, *344*, 1377−1380.

(16) Boles, M. A.; Engel, M.; Talapin, D. V. Self-Assembly of Colloidal Nanocrystals: From Intricate Structures to Functional Materials. *Chem. Rev.* **2016**, *116*, 11220−11289.

(17) Thomas, K. G.; Barazzouk, S.; Ipe, B. I.; Joseph, S. T. S.; Kamat, P. V. Uniaxial Plasmon Coupling through Longitudinal Self-Assembly of Gold Nanorods. *J. Phys. Chem. B* **2004**, *108*, 13066−13068.

(18) Gaponik, N.; Herrmann, A.-K.; Eychmüller, A. Colloidal Nanocrystal-Based Gels and Aerogels: Material Aspects and Application Perspectives. *J. Phys. Chem. Lett.* **2012**, *3*, 8−17.

(19) Singh, A.; Lindquist, B. A.; Ong, G. K.; Jadrich, R. B.; Singh, A.; Ha, H.; Ellison, C. J.; Truskett, T. M.; Milliron, D. J. Linking Semiconductor Nanocrystals into Gel Networks through All-Inorganic Bridges. *Angew. Chem., Int. Ed.* **2015**, *54*, 14840−14844.

(20) Lesnyak, V.; Voitekhovich, S. V.; Gaponik, P. N.; Gaponik, N.; Eychmüller, A. CdTe Nanocrystals Capped with a Tetrazolyl Analogue of Thioglycolic Acid: Aqueous Synthesis, Characterization, and Metal-Assisted Assembly. *ACS Nano* **2010**, *4*, 4090−4096.

(21) Sun, Y.; Harris, N. C.; Kiang, C.-H. The Reversible Phase Transition of DNA-Linked Colloidal Gold Assemblies. *Phys. A* **2005**, *354*, 1−9.

(22) Knorowski, C.; Travesset, A. Materials Design by DNA Programmed Self-Assembly. *Curr. Opin. Solid State Mater. Sci.* **2011**, *15*, 262−270.

(23) Macfarlane, R. J.; Lee, B.; Hill, H. D.; Senesi, A. J.; Seifert, S.; Mirkin, C. A. Assembly and Organization Processes in DNA-Directed Colloidal Crystallization. *Proc. Natl. Acad. Sci. U.S.A.* **2009**, *106*, 10493−10498.

(24) Borsley, S.; Kay, E. R. Dynamic Covalent Assembly and Disassembly of Nanoparticle Aggregates. *Chem. Commun.* **2016**, *52*, 9117−9120.

(25) Wang, Y.; Santos, P. J.; Kubiak, J. M.; Guo, X.; Lee, M. S.; Macfarlane, R. J. Multistimuli Responsive Nanocomposite Tectons for Pathway Dependent Self-Assembly and Acceleration of Covalent Bond Formation. *J. Am. Chem. Soc.* **2019**, *141*, 13234−13243.

(26) Hüsing, N.; Schubert, U. Aerogels—Airy Materials: Chemistry, Structure, and Properties. *Angew. Chem., Int. Ed.* **1998**, *37*, 22−45.

(27) Brinker, C. J.; Scherer, G. W. *Sol-Gel Science*; Academic Press: San Diego, 1990; pp 302−355.

(28) Nykypanchuk, D.; Maye, M. M.; van der Lelie, D.; Gang, O. DNA-Guided Crystallization of Colloidal Nanoparticles. *Nature* **2008**, *451*, 549−552.

(29) Park, S. Y.; Lytton-Jean, A. K. R.; Lee, B.; Weigand, S.; Schatz, G. C.; Mirkin, C. A. DNA-Programmable Nanoparticle Crystallization. *Nature* **2008**, *451*, 553−556.

(30) Hoppe, K.; Geidel, E.; Weller, H.; Eychmüller, A. Covalently Bound CdTe Nanocrystals. *Phys. Chem. Chem. Phys.* **2002**, *4*, 1704−1706.

(31) Maneeprakorn, W.; Malik, M. A.; O'Brien, P. Developing Chemical Strategies for the Assembly of Nanoparticles into Mesoscopic Objects. *J. Am. Chem. Soc.* **2010**, *132*, 1780−1781.

(32) Locatelli, E.; Ori, G.; Fournelle, M.; Lemor, R.; Montorsi, M.; Comes Franchini, M. Click Chemistry for the Assembly of Gold Nanorods and Silver Nanoparticles. *Chem.—Eur. J.* **2011**, *17*, 9052−9056.

(33) Liu, H.; Kumar, S. K.; Sciortino, F.; Evans, G. T. Vapor-Liquid Coexistence of Fluids with Attractive Patches: An Application of Wertheim's Theory of Association. *J. Chem. Phys.* **2009**, *130*, 044902.

https://dx.doi.org/10.1021/acs.chemmater.0c04151
Chem. Mater. 2020, 32, 10235−10245

(34) Russo, J.; Tartaglia, P.; Sciortino, F. Reversible Gels of Patchy Particles: Role of the Valence. *J. Chem. Phys.* **2009**, *131*, 014504.
(35) Pawar, A. B.; Kretzschmar, I. Fabrication, Assembly, and Application of Patchy Particles. *Macromol. Rapid Commun.* **2010**, *31*, 150−168.
(36) Howard, M. P.; Jadrich, R. B.; Lindquist, B. A.; Khabaz, F.; Bonnecaze, R. T.; Milliron, D. J.; Truskett, T. M. Structure and Phase Behavior of Polymer-Linked Colloidal Gels. *J. Chem. Phys.* **2019**, *151*, 124901.
(37) Luo, J.; Yuan, G.; Zhao, C.; Han, C. C.; Chen, J.; Liu, Y. Gelation of Large Hard Particles with Short-Range Attraction Induced by Bridging of Small Soft Microgels. *Soft Matter* **2015**, *11*, 2494−2503.
(38) Zhao, C.; Yuan, G.; Jia, D.; Han, C. C. Macrogel Induced by Microgel: Bridging and Depletion Mechanisms. *Soft Matter* **2012**, *8*, 7036−7043.
(39) Mayilo, S.; Hilhorst, J.; Susha, A. S.; Höhl, C.; Franzl, T.; Klar, T. A.; Rogach, A. L.; Feldmann, J. Energy Transfer in Solution-Based Clusters of CdTe Nanocrystals Electrostatically Bound by Calcium Ions. *J. Phys. Chem. C* **2008**, *112*, 14589−14594.
(40) Lindquist, B. A.; Jadrich, R. B.; Milliron, D. J.; Truskett, T. M. On the Formation of Equilibrium Gels via a Macroscopic Bond Limitation. *J. Chem. Phys.* **2016**, *145*, 074906.
(41) Sayevich, V.; Cai, B.; Benad, A.; Haubold, D.; Sonntag, L.; Gaponik, N.; Lesnyak, V.; Eychmüller, A. 3D Assembly of All-Inorganic Colloidal Nanocrystals into Gels and Aerogels. *Angew. Chem., Int. Ed.* **2016**, *55*, 6334−6338.
(42) Alivisatos, A. P.; Johnsson, K. P.; Peng, X.; Wilson, T. E.; Loweth, C. J.; Bruchez, M. P.; Schultz, P. G. Organization of "Nanocrystal Molecules" Using DNA. *Nature* **1996**, *382*, 609−611.
(43) Mirkin, C. A.; Letsinger, R. L.; Mucic, R. C.; Storhoff, J. J. A DNA-Based Method for Rationally Assembling Nanoparticles into Macroscopic Materials. *Nature* **1996**, *382*, 607−609.
(44) Xiong, H.; van der Lelie, D.; Gang, O. Phase Behavior of Nanoparticles Assembled by DNA Linkers. *Phys. Rev. Lett.* **2009**, *102*, 015504.
(45) Meadows, M. K.; Roesner, E. K.; Lynch, V. M.; James, T. D.; Anslyn, E. V. Boronic Acid Mediated Coupling of Catechols and N-Hydroxylamines: A Bioorthogonal Reaction to Label Peptides. *Org. Lett.* **2017**, *19*, 3179−3182.
(46) Rowan, S. J.; Cantrill, S. J.; Cousins, G. R. L.; Sanders, J. K. M.; Stoddart, J. F. Dynamic Covalent Chemistry. *Angew. Chem., Int. Ed.* **2002**, *41*, 898−952.
(47) Su, J.; Amamoto, Y.; Nishihara, M.; Takahara, A.; Otsuka, H. Reversible Cross-Linking of Hydrophilic Dynamic Covalent Polymers with Radically Exchangeable Alkoxyamines in Aqueous Media. *Polym. Chem.* **2011**, *2*, 2021−2026.
(48) Kay, E. R. Dynamic Covalent Nanoparticle Building Blocks. *Chem.—Eur. J.* **2016**, *22*, 10706−10716.
(49) Winne, J. M.; Leibler, L.; Du Prez, F. E. Dynamic Covalent Chemistry in Polymer Networks: A Mechanistic Perspective. *Polym. Chem.* **2019**, *10*, 6091−6108.
(50) Tian, Y.; Zhang, Y.; Wang, T.; Xin, H. L.; Li, H.; Gang, O. Lattice Engineering through Nanoparticle−DNA Frameworks. *Nat. Mater.* **2016**, *15*, 654−661.
(51) Imato, K.; Otsuka, H. Self-Healing of Polymers Based on Dynamic Covalent Chemistry. *Nippon Gazo Gakkaishi* **2015**, *54*, 221−228.
(52) An, Q.; Wessely, I. D.; Matt, Y.; Hassan, Z.; Bräse, S.; Tsotsalas, M. Recycling and Self-Healing of Dynamic Covalent Polymer Networks with a Precisely Tuneable Crosslinking Degree. *Polym. Chem.* **2019**, *10*, 672−678.
(53) Chen, C.-F.; Tzeng, S.-D.; Chen, H.-Y.; Lin, K.-J.; Gwo, S. Tunable Plasmonic Response from Alkanethiolate-Stabilized Gold Nanoparticle Superlattices: Evidence of Near-Field Coupling. *J. Am. Chem. Soc.* **2008**, *130*, 824−826.
(54) Barrow, S. J.; Wei, X.; Baldauf, J. S.; Funston, A. M.; Mulvaney, P. The Surface Plasmon Modes of Self-Assembled Gold Nanocrystals. *Nat. Commun.* **2012**, *3*, 1275.
(55) Funston, A. M.; Novo, C.; Davis, T. J.; Mulvaney, P. Plasmon Coupling of Gold Nanorods at Short Distances and in Different Geometries. *Nano Lett.* **2009**, *9*, 1651−1658.
(56) Liu, W.; Herrmann, A.-K.; Bigall, N. C.; Rodriguez, P.; Wen, D.; Oezaslan, M.; Schmidt, T. J.; Gaponik, N.; Eychmüller, A. Noble Metal Aerogels—Synthesis, Characterization, and Application as Electrocatalysts. *Acc. Chem. Res.* **2015**, *48*, 154−162.
(57) Wen, D.; Liu, W.; Haubold, D.; Zhu, C.; Oschatz, M.; Holzschuh, M.; Wolf, A.; Simon, F.; Kaskel, S.; Eychmüller, A. Gold Aerogels: Three-Dimensional Assembly of Nanoparticles and Their Use as Electrocatalytic Interfaces. *ACS Nano* **2016**, *10*, 2559−2567.
(58) Jansons, A. W.; Hutchison, J. E. Continuous Growth of Metal Oxide Nanocrystals: Enhanced Control of Nanocrystal Size and Radial Dopant Distribution. *ACS Nano* **2016**, *10*, 6942−6951.
(59) Reuther, J. F.; Dees, J. L.; Kolesnichenko, I. V.; Hernandez, E. T.; Ukraintsev, D. V.; Guduru, R.; Whiteley, M.; Anslyn, E. V. Dynamic Covalent Chemistry Enables Formation of Antimicrobial Peptide Quaternary Assemblies in a Completely Abiotic Manner. *Nat. Chem.* **2018**, *10*, 45−50.
(60) Weeks, J. D.; Chandler, D.; Andersen, H. C. Role of Repulsive Forces in Determining the Equilibrium Structure of Simple Liquids. *J. Chem. Phys.* **1971**, *54*, 5237−5247.
(61) Everaers, R.; Karimi-Varzaneh, H. A.; Fleck, F.; Hojdis, N.; Svaneborg, C. Kremer−Grest Models for Commodity Polymer Melts: Linking Theory, Experiment, and Simulation at the Kuhn Scale. *Macromolecules* **2020**, *53*, 1901−1916.
(62) Lee, H.; Venable, R. M.; Mackerell, A. D., Jr; Pastor, R. W. Molecular Dynamics Studies of Polyethylene Oxide and Polyethylene Glycol: Hydrodynamic Radius and Shape Anisotropy. *Biophys. J.* **2008**, *95*, 1590−1599.
(63) Swan, J. W.; Wang, G. Rapid Calculation of Hydrodynamic and Transport Properties in Concentrated Solutions of Colloidal Particles and Macromolecules. *Phys. Fluids* **2016**, *28*, 011902.
(64) Xing, Z.; Ness, C.; Frenkel, D.; Eiser, E. Structural and Linear Elastic Properties of DNA Hydrogels by Coarse-Grained Simulation. *Macromolecules* **2019**, *52*, 504−512.
(65) Wertheim, M. S. Fluids with Highly Directional Attractive Forces. III. Multiple Attraction Sites. *J. Stat. Phys.* **1986**, *42*, 459−476.
(66) Wertheim, M. S. Fluids with Highly Directional Attractive Forces. IV. Equilibrium Polymerization. *J. Stat. Phys.* **1986**, *42*, 477−492.
(67) Chapman, W. G.; Jackson, G.; Gubbins, K. E. Phase Equilibria of Associating Fluids. *Mol. Phys.* **1988**, *65*, 1057−1079.
(68) Amos, M. D.; Jackson, G. Bonded Hard-sphere (BHS) Theory for the Equation of State of Fused Hard-sphere Polyatomic Molecules and Their Mixtures. *J. Chem. Phys.* **1992**, *96*, 4604−4618.
(69) Boublík, T. Hard-Sphere Equation of State. *J. Chem. Phys.* **1970**, *53*, 471−472.
(70) Plimpton, S. Fast Parallel Algorithms for Short-Range Molecular Dynamics. *J. Comput. Phys.* **1995**, *117*, 1−19.
(71) Chan, W.; White, P. D. *Fmoc Solid-Phase Peptide Synthesis: A Practical Approach*; Oxford University Press: England, 2000; Vol. *222*.
(72) Hawker, C. J.; Fokin, V. V.; Finn, M. G.; Sharpless, K. B. Bringing Efficiency to Materials Synthesis: The Philosophy of Click Chemistry. *Aust. J. Chem.* **2007**, *60*, 381−383.
(73) Reuther, J. F.; Dahlhauser, S. D.; Anslyn, E. V. Tunable Orthogonal Reversible Covalent (TORC) Bonds: Dynamic Chemical Control over Molecular Assembly. *Angew. Chem., Int. Ed.* **2019**, *58*, 74−85.
(74) Reuther, J. F.; Goodrich, A. C.; Escamilla, P. R.; Lu, T. A.; Del Rio, V.; Davies, B. W.; Anslyn, E. V. A Versatile Approach to Noncanonical, Dynamic Covalent Single- and Multi-Loop Peptide Macrocycles for Enhancing Antimicrobial Activity. *J. Am. Chem. Soc.* **2018**, *140*, 3768−3774.
(75) Stewart, M. H.; Susumu, K.; Mei, B. C.; Medintz, I. L.; Delehanty, J. B.; Blanco-Canosa, J. B.; Dawson, P. E.; Mattoussi, H. Multidentate Poly(Ethylene Glycol) Ligands Provide Colloidal Stability to Semiconductor and Metallic Nanocrystals in Extreme Conditions. *J. Am. Chem. Soc.* **2010**, *132*, 9804−9813.

https://dx.doi.org/10.1021/acs.chemmater.0c04151
Chem. Mater. 2020, 32, 10235−10245

(76) Kairdolf, B. A.; Nie, S. Multidentate-Protected Colloidal Gold Nanocrystals: PH Control of Cooperative Precipitation and Surface Layer Shedding. *J. Am. Chem. Soc.* **2011**, *133*, 7268−7271.
(77) Zhang, Y.; Clapp, A. Overview of Stabilizing Ligands for Biocompatible Quantum Dot Nanocrystals. *Sensors* **2011**, *11*, 11036−11055.
(78) Seifert, H. M.; Ramirez Trejo, K.; Anslyn, E. V. Four Simultaneously Dynamic Covalent Reactions. Experimental Proof of Orthogonality. *J. Am. Chem. Soc.* **2016**, *138*, 10916−10924.
(79) Majetich, S. A.; Carter, A. C.; Belot, J.; McCullough, R. D. ^{1}H NMR Characterization of the CdSe Nanocrystallite Surface. *J. Phys. Chem.* **1994**, *98*, 13705−13710.
(80) Fritzinger, B.; Capek, R. K.; Lambert, K.; Martins, J. C.; Hens, Z. Utilizing Self-Exchange To Address the Binding of Carboxylic Acid Ligands to CdSe Quantum Dots. *J. Am. Chem. Soc.* **2010**, *132*, 10195−10201.
(81) Moreels, I.; Fritzinger, B.; Martins, J. C.; Hens, Z. Surface Chemistry of Colloidal PbSe Nanocrystals. *J. Am. Chem. Soc.* **2008**, *130*, 15081−15086.
(82) De Roo, J.; Justo, Y.; De Keukeleere, K.; Van den Broeck, F.; Martins, J. C.; Van Driessche, I.; Hens, Z. Carboxylic-Acid-Passivated Metal Oxide Nanocrystals: Ligand Exchange Characteristics of a New Binding Motif. *Angew. Chem., Int. Ed.* **2015**, *54*, 6488−6491.
(83) Hens, Z.; Martins, J. C. A Solution NMR Toolbox for Characterizing the Surface Chemistry of Colloidal Nanocrystals. *Chem. Mater.* **2013**, *25*, 1211−1221.
(84) Agrawal, A.; Singh, A.; Yazdi, S.; Singh, A.; Ong, G. K.; Bustillo, K.; Johns, R. W.; Ringe, E.; Milliron, D. J. Resonant Coupling between Molecular Vibrations and Localized Surface Plasmon Resonance of Faceted Metal Oxide Nanocrystals. *Nano Lett.* **2017**, *17*, 2611−2620.
(85) Jain, P. K.; Lee, K. S.; El-Sayed, I. H.; El-Sayed, M. A. Calculated Absorption and Scattering Properties of Gold Nanoparticles of Different Size, Shape, and Composition: Applications in Biological Imaging and Biomedicine. *J. Phys. Chem. B* **2006**, *110*, 7238−7248.
(86) Lassiter, J. B.; Aizpurua, J.; Hernandez, L. I.; Brandl, D. W.; Romero, I.; Lal, S.; Hafner, J. H.; Nordlander, P.; Halas, N. J. Close Encounters between Two Nanoshells. *Nano Lett.* **2008**, *8*, 1212−1218.
(87) Ruzicka, B.; Zaccarelli, E.; Zulian, L.; Angelini, R.; Sztucki, M.; Moussaïd, A.; Narayanan, T.; Sciortino, F. Observation of Empty Liquids and Equilibrium Gels in a Colloidal Clay. *Nat. Mater.* **2011**, *10*, 56−60.
(88) Li, T.; Senesi, A. J.; Lee, B. Small Angle X-Ray Scattering for Nanoparticle Research. *Chem. Rev.* **2016**, *116*, 11128−11180.
(89) Bauer, P. S.; Amenitsch, H.; Baumgartner, B.; Köberl, G.; Rentenberger, C.; Winkler, P. M. In-Situ Aerosol Nanoparticle Characterization by Small Angle X-Ray Scattering at Ultra-Low Volume Fraction. *Nat. Commun.* **2019**, *10*, 1122.
(90) Jullien, R.; Kolb, M. Hierarchical Model for Chemically Limited Cluster-Cluster Aggregation. *J. Phys. A: Math. Gen.* **1984**, *17*, L639−L643.
(91) Nishi, K.; Shibayama, M. Probe-SAXS on Hydrogels under Elongation. *Soft Matter* **2016**, *12*, 5334−5339.
(92) Lazzari, S.; Nicoud, L.; Jaquet, B.; Lattuada, M.; Morbidelli, M. Fractal-like Structures in Colloid Science. *Adv. Colloid Interface Sci.* **2016**, *235*, 1−13.
(93) Lattuada, M.; Wu, H.; Hasmy, A.; Morbidelli, M. Estimation of Fractal Dimension in Colloidal Gels. *Langmuir* **2003**, *19*, 6312−6316.
(94) Beaucage, G. Small-Angle Scattering from Polymeric Mass Fractals of Arbitrary Mass-Fractal Dimension. *J. Appl. Crystallogr.* **1996**, *29*, 134−146.
(95) Lin, M. Y.; Lindsay, H. M.; Weitz, D. A.; Ball, R. C.; Klein, R.; Meakin, P. Universality in Colloid Aggregation. *Nature* **1989**, *339*, 360−362.
(96) Tang, S.; Preece, J. M.; McFarlane, C. M.; Zhang, Z. Fractal Morphology and Breakage of DLCA and RLCA Aggregates. *J. Colloid Interface Sci.* **2000**, *221*, 114−123.
(97) Tandon, B.; Agrawal, A.; Heo, S.; Milliron, D. J. Competition between Depletion Effects and Coupling in the Plasmon Modulation of Doped Metal Oxide Nanocrystals. *Nano Lett.* **2019**, *19*, 2012−2019.
(98) Agrawal, A.; Johns, R. W.; Milliron, D. J. Control of Localized Surface Plasmon Resonances in Metal Oxide Nanocrystals. *Annu. Rev. Mater. Res.* **2017**, *47*, 1−31.
(99) Abb, M.; Wang, Y.; Papasimakis, N.; de Groot, C. H.; Muskens, O. L. Surface-Enhanced Infrared Spectroscopy Using Metal Oxide Plasmonic Antenna Arrays. *Nano Lett.* **2014**, *14*, 346−352.
(100) Jain, P. K.; El-Sayed, M. A. Plasmonic Coupling in Noble Metal Nanostructures. *Chem. Phys. Lett.* **2010**, *487*, 153−164.
(101) Kool, E. T.; Park, D.-H.; Crisalli, P. Fast Hydrazone Reactants: Electronic and Acid/Base Effects Strongly Influence Rate at Biological PH. *J. Am. Chem. Soc.* **2013**, *135*, 17663−17666.
(102) Dirksen, A.; Dawson, P. E. Rapid Oxime and Hydrazone Ligations with Aromatic Aldehydes for Biomolecular Labeling. *Bioconjugate Chem.* **2008**, *19*, 2543−2548.
(103) Kress, R. N.; Jones, M. R. Colloidal Interactions Get Patchy and Directional. *Proc. Natl. Acad. Sci. U.S.A.* **2020**, *117*, 15382−15384.
(104) Sun, X.; Chwatko, M.; Lee, D.-H.; Bachman, J. L.; Reuther, J. F.; Lynd, N. A.; Anslyn, E. V. Chemically Triggered Synthesis, Remodeling, and Degradation of Soft Materials. *J. Am. Chem. Soc.* **2020**, *142*, 3913−3922.
(105) Higaki, Y.; Otsuka, H.; Takahara, A. A Thermodynamic Polymer Cross-Linking System Based on Radically Exchangeable Covalent Bonds. *Macromolecules* **2006**, *39*, 2121−2125.
(106) Jin, Y.; Yu, C.; Denman, R. J.; Zhang, W. Recent Advances in Dynamic Covalent Chemistry. *Chem. Soc. Rev.* **2013**, *42*, 6634−6654.
(107) Rogers, W. B.; Manoharan, V. N. Programming Colloidal Phase Transitions with DNA Strand Displacement. *Science* **2015**, *347*, 639−642.

https://dx.doi.org/10.1021/acs.chemmater.0c04151
Chem. Mater. 2020, 32, 10235−10245